Vol 463|7 January 2010|doi:10.1038/nature08652

LETTERS

High-performance genetically targetable optical neural silencing by light-driven proton pumps

Brian Y. Chow[1,2]*, Xue Han[1,2]*, Allison S. Dobry[1,2], Xiaofeng Qian[1,2], Amy S. Chuong[1,2], Mingjie Li[1,2], Michael A. Henninger[1,2], Gabriel M. Belfort[2], Yingxi Lin[2], Patrick E. Monahan[1,2] & Edward S. Boyden[1,2]

The ability to silence the activity of genetically specified neurons in a temporally precise fashion would provide the opportunity to investigate the causal role of specific cell classes in neural computations, behaviours and pathologies. Here we show that members of the class of light-driven outward proton pumps can mediate powerful, safe, multiple-colour silencing of neural activity. The gene archaerhodopsin-3 (Arch)[1] from *Halorubrum sodomense* enables near-100% silencing of neurons in the awake brain when virally expressed in the mouse cortex and illuminated with yellow light. Arch mediates currents of several hundred picoamps at low light powers, and supports neural silencing currents approaching 900 pA at light powers easily achievable *in vivo*. Furthermore, Arch spontaneously recovers from light-dependent inactivation, unlike light-driven chloride pumps that enter long-lasting inactive states in response to light. These properties of Arch are appropriate to mediate the optical silencing of significant brain volumes over behaviourally relevant timescales. Arch function in neurons is well tolerated because pH excursions created by Arch illumination are minimized by self-limiting mechanisms to levels comparable to those mediated by channelrhodopsins[2,3] or natural spike firing. To highlight how proton pump ecological and genomic diversity may support new innovation, we show that the blue–green light-drivable proton pump from the fungus *Leptosphaeria maculans*[4] (Mac) can, when expressed in neurons, enable neural silencing by blue light, thus enabling alongside other developed reagents the potential for independent silencing of two neural populations by blue versus red light. Light-driven proton pumps thus represent a high-performance and extremely versatile class of 'optogenetic' voltage and ion modulator, which will broadly enable new neuroscientific, biological, neurological and psychiatric investigations.

We screened type I microbial opsins (see Supplementary Table 1) from archaebacteria, bacteria, plants and fungi for light-driven hyperpolarizing capability[5]. Mammalian codon-optimized genes were synthesized, cloned into green fluorescent protein (GFP)-fusion expression vectors, and transfected into cultured neurons. We measured opsin photocurrents and cell capacitance-normalized photocurrent densities under stereotyped illumination conditions (Fig. 1a, black and grey bars, respectively), as well as opsin action spectra (photocurrent as a function of wavelength; Supplementary Table 2). From this information, we estimated the photocurrent density for each opsin at its own spectral peak (Fig. 1a, white bars). For comparison purposes, we included an earlier-characterized microbial opsin, the *Natronomonas pharaonis* halorhodopsin (Halo/NpHR)—a light-driven inward chloride pump capable of modest hyperpolarizing currents[6–9]. Archaerhodopsin-3 from *H. sodomense* (Arch/aR-3), proposed to be a proton pump[1], generated large photocurrents in the screen, as did two other proton pumps, the *Leptosphaeria maculans* opsin (Mac/LR/Ops)[4] and cruxrhodopsin-1 (ref. 10) (albeit less than that of Arch; Fig. 1a). All light-driven chloride pumps assessed had lower screen photocurrents than these light-driven proton pumps.

Arch is a yellow–green light-sensitive (Fig. 1b) opsin that seems to express well on the neural plasma membrane (Fig. 1c; see Supplementary Notes on Arch expression levels and enhancing Arch membrane trafficking). Arch-mediated currents exhibited excellent kinetics of light-activation and post-light recovery. After illumination, Arch currents rose with a 15–85% onset time of 8.8 ± 1.8 ms (mean $\pm$ standard error (s.e.) reported throughout, unless otherwise indicated; $n = 16$ neurons), and after light cessation, Arch currents fell with an 85–15% offset time of 19.3 ± 2.9 ms. Under continuous yellow illumination, Arch photocurrent declined (Fig. 1d, e), as did the photocurrents of all of the opsins in our screen. However, unlike all of the halorhodopsins we screened (including products of halorhodopsin site-directed mutagenesis aimed at improving kinetics; Supplementary Table 3), which after illumination remained inactivated for long periods of time (for example, tens of minutes, with accelerated recovery requiring more blue light[6,11]), Arch spontaneously recovered function in seconds (Fig. 1d, e), more like the light-gated cation channel channelrhodopsin-2 from *Chlamydomonas reinhardtii* (ChR2)[2,3]. The magnitude of Arch-mediated photocurrents was large. At low light irradiances of 0.35 and 1.28 mW mm^{-2} (Fig. 1f, left), neural Arch currents were 120 and 189 pA, respectively; at higher light powers (for example, at which Halo currents saturate), Arch currents continued to increase, approaching 900 pA at effective irradiances of 36 mW mm^{-2}, well within the reach of typical *in vivo* experiments (Fig. 1f, right; see Methods for how effective irradiances were calculated). The high dynamic range of Arch may enable the use of light sources (for example, light-emitting diodes (LEDs), lasers) that are safe and effective for optical control *in vivo*[12,13].

Several lines of evidence supported the idea that Arch functioned as an outward proton pump when expressed in neurons. Removing the endogenous ions that commonly subserve neural inhibition, Cl^- and K^+, from physiological solutions did not alter photocurrent magnitude ($P > 0.4$ comparing either K^+-free or Cl^--free solutions to regular solutions, *t*-test; Fig. 2a). In solutions lacking Na^+, K^+, Cl^- and Ca^{2+}, photocurrents were still no different from those measured in normal solutions ($P > 0.4$; $n = 4$ neurons tested without these four charge carriers). The reversal potential appeared to be less than -120 mV (Fig. 2b), also consistent with Arch being a proton pump.

We assessed the voltage swings driven by illumination of current-clamped Arch-expressing cultured neurons. As effective irradiance increased from 7.8 mW mm^{-2} to 36.3 mW mm^{-2} (Fig. 1f), voltage-clamped neurons exhibited peak currents that increased from

[1]The MIT Media Laboratory, Synthetic Neurobiology Group, and Department of Biological Engineering, [2]Department of Brain and Cognitive Sciences and MIT McGovern Institute for Brain Research, Massachusetts Institute of Technology, Cambridge, Massachusetts 02139, USA.
*These authors contributed equally to this work.

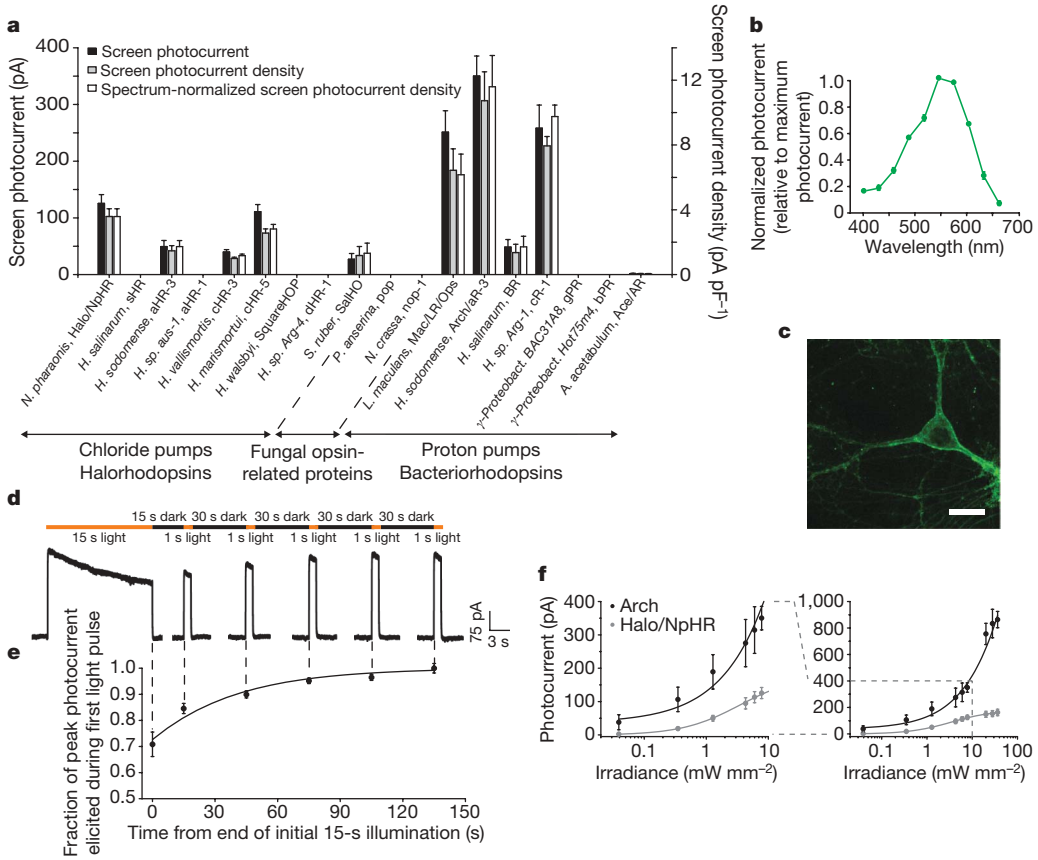

Figure 1 | Optical neural silencing by light-driven proton pumping, revealed by a cross-kingdom functional molecular screen. a, Screen data showing outward photocurrents (left *y* axis, black bars), photocurrent densities (right *y* axis, grey bars), and action spectrum-normalized photocurrent densities (right *y* axis, white bars), measured by whole-cell patch-clamp of cultured neurons under screening illumination conditions (575 ± 25 nm, 7.8 mW mm^{-2} for all except Mac/LR/Ops, gPR, bPR and Ace/AR, which were 535 ± 25 nm, 9.4 mW mm^{-2}; see Supplementary Table 1 for details on the molecules screened; $n = 4$–16 neurons for each bar). Data are mean and s.e. Full species names from left to right: *Natronomonas pharaonis*, *Halobacterium salinarum*, *Halorubrum sodomense*, *Halorubrum species aus-1*, *Haloarcula vallismortis*, *Haloarcula marismortui*, *Haloquadratum walsbyi*, *Haloterrigena species Arg-4*, *Salinibacter ruber*, *Podospora anserina*, *Neurospora crassa*, *Leptosphaeria maculans*, *Halorubrum sodomense*, *Halobacterium salinarum*, *Haloarcula species Arg-1*, *uncultured gamma-proteobacterium BAC31A8*, *uncultured gamma-proteobacterium Hot75m4* and *Acetabularia acetabulum*[5]. **b**, Action spectrum of Arch measured in cultured neurons by scanning illumination light wavelength through the visible spectrum ($n = 7$ neurons). **c**, Confocal fluorescence image of a lentivirally infected cultured neuron expressing Arch–GFP. Scale bar, 20 μm. **d**, Raw current trace of a neuron lentivirally infected with Arch, illuminated by a 15-s light pulse (575 ± 25 nm, irradiance 7.8 mW mm^{-2}) followed by 1-s test pulses delivered at 15, 45, 75, 105 and 135 s after the end of the 15-s light pulse. **e**, Population data of averaged Arch photocurrents ($n = 11$ neurons) sampled at the times indicated by the vertical dotted lines that extend into **d**. **f**, Photocurrents of Arch versus Halo measured as a function of 575 ± 25 nm light irradiance (or effective light irradiance; see Methods for details), in patch-clamped cultured neurons ($n = 4$–16 neurons for each point), for low (left) and high (right) light powers. The line is a single Hill fit to the data.

350 ± 35 pA ($n = 16$ neurons) to 863 ± 62 pA ($n = 8$ neurons), respectively. Current-clamped neurons under these two irradiance conditions were hyperpolarized by −69.6 ± 7.3 mV ($n = 10$) and −76.2 ± 10.1 mV ($n = 8$), respectively. Notably, these voltage deflections, although both large, were not significantly different from one another ($P > 0.7$, *t*-test), suggesting the existence of a rapidly activated transporter or exchanger (perhaps the Na^+-dependent Cl^-/HCO_3^- exchanger), or the opening of hyperpolarization-gated channels capable of shunting protons, which limit the effects of Arch on accumulated proton (or other charge carrier) gradients across neural membranes. This enabling of effective but not excessive silencing may make Arch safer than pumps that accumulate ions without self-regulation.

We next assessed the changes in intracellular pH (pH_i) driven by illumination of Arch-expressing cultured neurons, using the fluorescent pH indicator carboxy-SNARF-1. Within 1 s of illumination with strong green light (Fig. 2c), pH_i rose from 7.309 ± 0.011 to 7.431 ± 0.020, plateauing rapidly. pH_i increased slightly further after 15 s of illumination to 7.461 ± 0.024 (Fig. 1e). The fast stabilization of pH_i may reflect the same self-limiting influence that limits proton-mediated voltage swings as described earlier, and may contribute to the safe operation of Arch in neurons by preventing large pH_i swings. The changes in pH_i observed here are comparable in magnitude to those observed during illumination of ChR2-expressing cells[14] (owing to the proton currents carried by ChR2; refs 3, 15), and are also within the magnitudes of changes observed during normal neural activity[16–19]. Passive electrical properties of neurons were not affected by Arch expression (Fig. 2e–g; $P > 0.6$ for each measure, *t*-test), nor was cell death ($P > 0.6$, $\chi^2 = 0.26$; Fig. 2d).

We estimated the tissue volumes that could be silenced, using *in vitro* experiments and computational modelling. In cultured neurons expressing Arch or a trafficking-improved variant of Halo, eNpHR[8,9], we somatically injected brief current pulses at magnitudes chosen to mimic the current drives of neurons in the intact nervous system[20–23]. We exposed these neurons to periods of 575 nm yellow light (0.35, 1.28 or 6 mW mm^{-2}, simulating irradiance ~1.7, 1.2 or 0.6 mm away from the tip of a 200-μm fibre emitting 200 mW mm^{-2} irradiance, as modelled by Monte Carlo methods; see Supplementary Fig. 3), and measured the reduction in spike rate for each condition (Fig. 3a). In general, Arch-expressing neurons were significantly more inhibited than eNpHR-expressing cells. According to our model and the 350 pA data in Fig. 3a, the increase in brain tissue volume that would be 45–55% optically silenced would be ~10 times larger for Arch than for eNpHR.

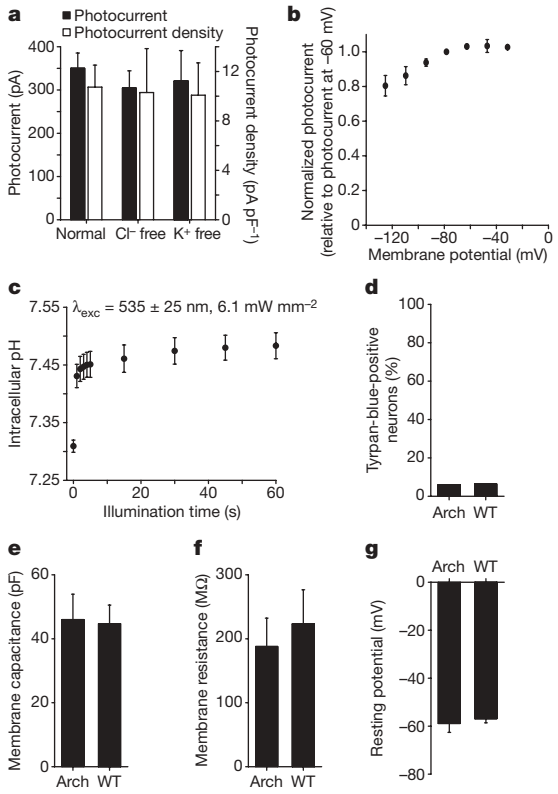

Figure 2 | Functional properties of the light-driven proton pump Arch in neurons. **a**, Photocurrent of Arch measured as a function of ionic composition (575 ± 25 nm light, 7.8 mW mm^{-2}), showing no significant dependence of photocurrent on the concentration of Cl^- or K^+ ions in bath and intracellular solutions (n = 16, 8 and 7 neurons, from left to right). **b**, Arch proton photocurrent versus holding potential (n = 4 neurons). **c**, Intracellular pH measurements over a 1-min period of continuous illumination and simultaneous imaging (535 ± 25 nm light, 6.1 mW mm^{-2}) using SNARF-1 pH-sensitive ratiometric dye (n = 10–20 cells per data point). **d**, Trypan-blue staining of neurons lentivirally infected with Arch versus wild-type (WT) neurons, measured at 18 days *in vitro* (n = 669 Arch-expressing, 512 wild-type neurons). **e–g**, Membrane capacitance (**e**), membrane resistance (**f**), and resting potential (**g**) in neurons lentivirally infected with Arch versus wild-type neurons, measured at 11 days *in vitro* (n = 7 cells each).

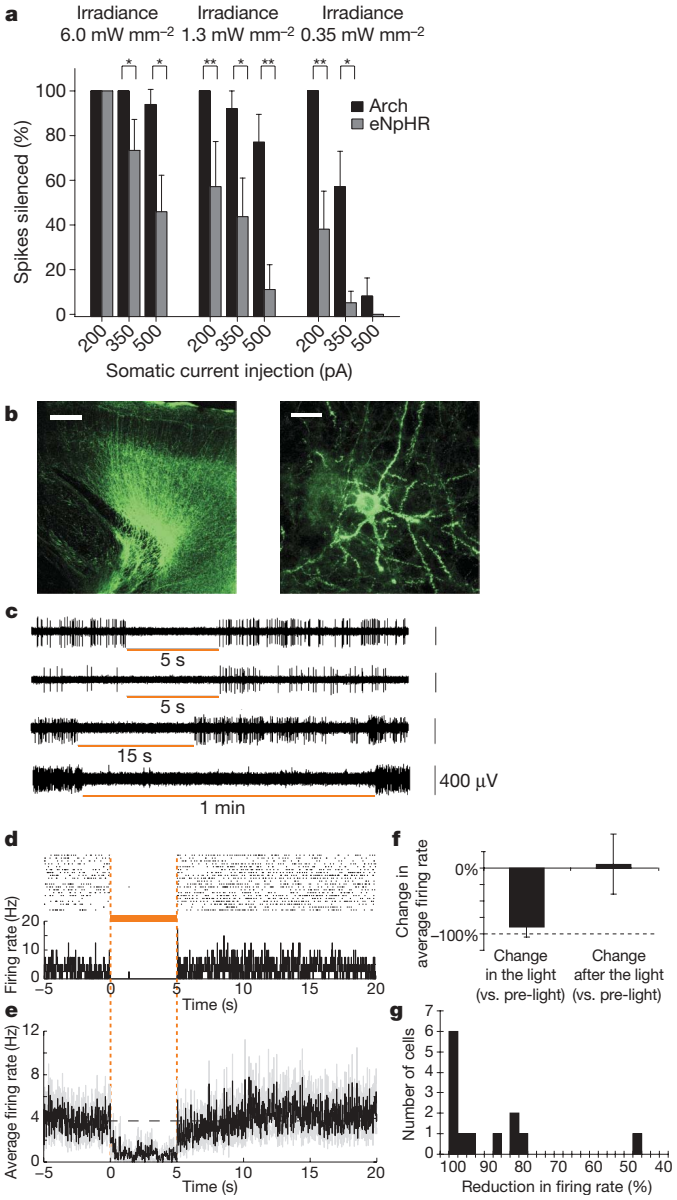

Figure 3 | High-performance Arch-mediated optical neural silencing of neocortical regions in awake mice. **a**, *In vitro* data showing, in cultured neurons expressing Arch or eNpHR and receiving trains of somatic current injections (15-ms pulse durations at 5 Hz), the per cent reduction of spiking under varying light powers (575 ± 25 nm light) as might be encountered *in vivo*. *P < 0.05, **P < 0.01, t-test. n = 7–8 cells for each condition. **b**, Fluorescence images showing Arch–GFP expression in mouse cortex ~1 month after lentiviral (FCK–Arch–GFP) injection. Scale bars, 200 μm (left) and 20 μm (right). **c**, Representative extracellular recordings showing neurons undergoing 5-s, 15-s and 1-min periods of light illumination (593 nm; ~150 mW mm^{-2} radiant flux out the fibre tip; and expected to be ~3 mW mm^{-2} at the electrode tip ~800 μm away[12,13,24]). **d**, Neural activity in a representative neuron before, during and after 5 s of yellow light illumination, shown as a spike raster plot (top), and as a histogram of instantaneous firing rate averaged across trials (bottom; bin size, 20 ms). **e**, Population average of instantaneous firing rate before, during and after yellow light illumination (black line, mean; grey lines, mean ± s.e.; n = 13 units). **f**, Average change in spike firing during 5-s of yellow light illumination (left) and during the 5 s immediately after light offset (right), for the data shown in **d**. **g**, Histogram of percentage reductions in spike rate, for each individual neuron, integrated across all 5-s silencing period.

To assess Arch *in vivo* directly, we injected lentivirus encoding for Arch into mouse cortex and recorded neural responses ~1 month later. Arch expressed well (Fig. 3b, left) and appeared well localized to the plasma membrane, labelling cell bodies, processes and dendritic spines (Fig. 3b, right). We recorded neurons in awake head-fixed mice, illuminating neurons by a 200-μm optical fibre coupled to a 593-nm laser (power at electrode tip estimated at ~3 mW mm^{-2}; refs 12, 13, 24). After light onset, firing rates of many units immediately and strongly declined, and remained low throughout the period of illumination, for both brief (Fig. 3c, top, d) and long (Fig. 3c, bottom) pulses. We recorded 13 single units that showed any decrease in firing during illumination, objectively identified as described in the Methods, and found spiking rates during exposure to 5 s yellow light (Fig. 3d) to drop by an average of 90 ± 15% (mean ± s.d.; Fig. 3e, f), restoring to levels indistinguishable from baseline after light cessation (P > 0.2, paired t-test; Fig. 3f). Six of the 13 units decreased spike rate by at least 99.5%, and the median decrease was 97.1% (Fig. 3g). One possibility is that Arch-expressing cells were almost completely silenced, whereas non-infected cells decreased activity owing to network activity reduction during illumination; note that only excitatory cells were genetically targeted here. Optical silencing was consistent across trials (P > 0.1, paired t-test comparing, for each neuron, responses to the first three versus the last three light exposures; ~20 trials per neuron). The kinetics of silencing were rapid: for the six neurons that underwent >99.5% silencing, spike firing reduced with near-0-ms latency, rarely firing spikes after light onset; averaged across all cells, firing-rate reductions plateaued within 229 ± 310 ms (mean ± s.d.) after light onset. After light cessation, firing rate restored quickly for

the highly silenced neurons; averaged across all cells, firing rates took 355 ± 505 ms to recover after light offset. The level of post-light firing did not vary with repeated light exposure ($P > 0.7$, paired t-test comparing, for each neuron, after-light firing rates during the first three versus the last three trials). Thus, Arch could mediate reliable, near-digital silencing of neurons in the awake mammalian brain.

Proton pumps naturally exist that are activated by many colours of light (see Supplementary Table 1), in contrast to chloride pumps, which are primarily driven by yellow–orange light (even with significant mutagenesis of retinal-flanking residues; Supplementary Table 3). The light-driven proton pump Mac (Fig. 1a), in our screen, had an action spectrum strongly blueshifted relative to that of the light-driven chloride pump Halo (Fig. 4a). We found that Mac-expressing neurons could undergo 4.1-fold larger hyperpolarizations with blue light than with red light, and Halo-expressing neurons could undergo 3.3-fold larger hyperpolarizations with red light than with blue light, when illuminated with appropriate filters (Fig. 4b). Accordingly, we could demonstrate selective silencing of spike firing in Mac-expressing neurons in response to blue light, and selective silencing of spike firing in Halo-expressing neurons in response to red light (Fig. 4c). Thus, the spectral diversity of proton pumps points the way towards independent multicolour silencing of separate neural populations. This result opens up new kinds of experiment, in which, for example, two neuron classes, or two sets of neural projections from a single site, can be independently silenced during a behavioural task.

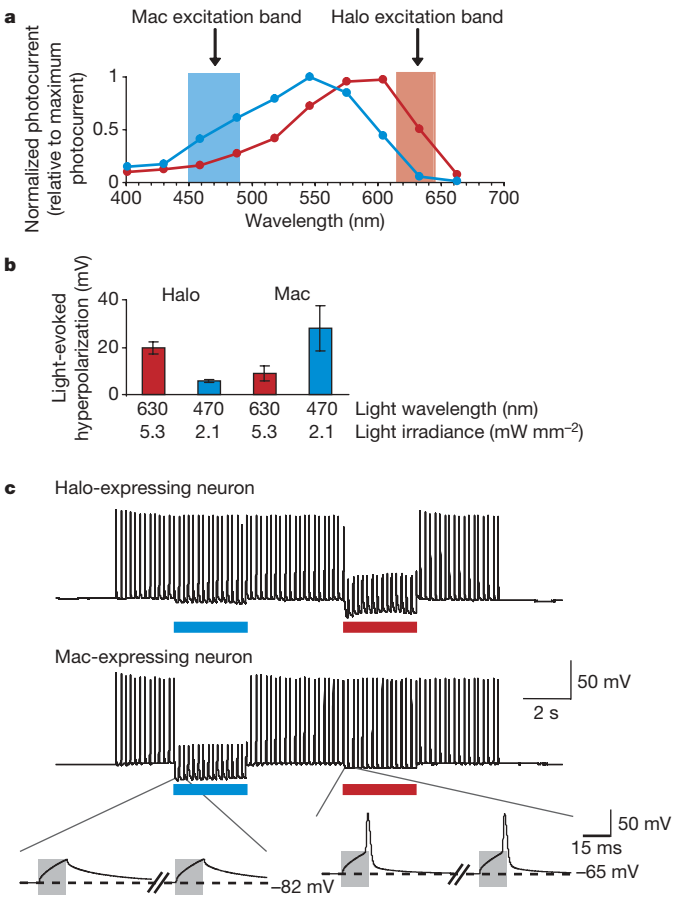

Figure 4 | Multicolour silencing of two neural populations, enabled by blue- and red-light drivable ion pumps of different classes. a, Action spectra of Mac versus Halo; rectangles indicate filter bandwidths used for multicolour silencing *in vitro*. Blue light is delivered by a 470 ± 20 nm filter at 5.3 mW mm^{-2}, and red light is delivered by a 630 ± 15 nm filter at 2.1 mW mm^{-2}. **b**, Membrane hyperpolarizations elicited by blue versus red light, in cells expressing Halo or Mac ($n = 5$ Mac-expressing and $n = 6$ Halo-expressing neurons). **c**, Action potentials evoked by current injection into patch-clamped cultured neurons transfected with Halo (top) were selectively silenced by the red light but not by the blue light, and vice-versa in neurons expressing Mac (middle). Grey boxes in the inset (bottom) indicate periods of patch-clamp current injection.

Arch and Mac represent members of a new, diverse and powerful class of optical neural silencing reagent, the light-driven proton pump, which operates without the need for exogenous chemical supplementation in mammalian cells. The efficacy of these proton pumps is surprising, given that protons occur, in mammalian tissue, at a million-fold lower concentration than the ions carried by other optical control molecules. This high efficacy may be due to the fast photocycle of Arch (see also refs 25, 26), but it may also be due to the ability of high-pK_a residues in proton pumps to mediate proton uptake[25,27]. We discovered several facts about this class of molecules that point the way for future neuroengineering innovation. First, proton pumping is a self-limiting process in neurons, providing for a safe and naturalistic form of neural silencing. Second, proton pumps recover spontaneously after optical activation, improving their relevance for behaviourally relevant silencing over the class of halorhodopsins. Finally, proton pumps exist with a wide diversity of action spectra, thus enabling multiple-colour silencing of distinct neural populations. Structure-guided mutagenesis of Arch and Mac may further facilitate development of neural silencers with altered spectrum or ion selectivity, given the significant amount of structure–function knowledge of the proton pump family (for example, refs 28–30).

Our study highlights the importance of ecological and genomic diversity in providing new molecular reagents for optical control of biological processes, as has previously benefited the fluorescent protein community. These opsins are likely to find uses across the spectrum of neuroscientific, biological and bioengineering fields. For example, expression of these opsins in neurons, muscle, immune cells and other excitable cells will allow control over their membrane potential, providing the opportunity to investigate the causal role of specific cells' activities in intact organisms, and, potentially, to understand the causal contribution of such cells to disease states in animal models. With the recent demonstration of the safe and efficacious use of the microbial opsin ChR2 to control neurons in non-human primates[24], it is in principle possible that in the future, these opsins may subserve new forms of neuromodulation technology that bear clinical benefit.

METHODS SUMMARY

Constructs with Arch, Mac and Halo are available at http://syntheticneurobiology.org/protocols. In brief, codon-optimized genes were synthesized by Genscript and fused to GFP in lentiviral and mammalian expression vectors as used previously[6,24] for transfection or viral infection of neurons. Primary hippocampal or cortical neurons were cultured and then transfected with plasmids or infected with viruses encoding for genes of interest, as described previously[6]. Images were taken using a Zeiss LSM 510 confocal microscope. Patch-clamp recordings were made using glass microelectrodes and a Multiclamp 700B/Digidata electrophysiology setup, using appropriate pipette and bath solutions for the experimental goal at hand. Neural pH imaging was done using carboxy-SNARF-1-AM ester (Invitrogen). Cell health was assayed using trypan blue staining (Gibco). HEK cells were cultured and patch-clamped using standard protocols. Mutagenesis was performed using the QuikChange kit (Stratagene). Computational modelling of light propagation was done with Monte Carlo simulation with MATLAB. *In vivo* recordings were made on head-fixed awake mice, which were surgically injected with lentivirus, and implanted with a headplate as described before[24]. Glass pipettes attached to laser-coupled optical fibres were inserted into the brain, to record neural activity during laser illumination in a photoelectrochemical artefact-free way. Data analysis was performed using Clampfit, Excel, Origin and MATLAB. Histology was performed using transcardial formaldehyde perfusion followed by sectioning and subsequent confocal imaging.

Received 27 August; accepted 9 November 2009.

1. Ihara, K. *et al.* Evolution of the archaeal rhodopsins: evolution rate changes by gene duplication and functional differentiation. *J. Mol. Biol.* **285**, 163–174 (1999).
2. Boyden, E. S., Zhang, F., Bamberg, E., Nagel, G. & Deisseroth, K. Millisecond-timescale, genetically targeted optical control of neural activity. *Nature Neurosci.* **8**, 1263–1268 (2005).

3. Nagel, G. *et al.* Channelrhodopsin-2, a directly light-gated cation-selective membrane channel. *Proc. Natl Acad. Sci. USA* **100,** 13940–13945 (2003).
4. Waschuk, S. A., Bezerra, A. G., Shi, L. & Brown, L. S. Leptosphaeria rhodopsin: Bacteriorhodopsin-like proton pump from a eukaryote. *Proc. Natl Acad. Sci. USA* **102,** 6879–6883 (2005).
5. Klare, J. P., Chizhov, I. & Engelhard, M. Microbial rhodopsins: scaffolds for ion pumps, channels, and sensors. *Results Probl. Cell Differ.* **45,** 73–122 (2008).
6. Han, X. & Boyden, E. S. Multiple-color optical activation, silencing, and desynchronization of neural activity, with single-spike temporal resolution. *PLoS One* **2,** e299 (2007).
7. Zhang, F. *et al.* Multimodal fast optical interrogation of neural circuitry. *Nature* **446,** 633–639 (2007).
8. Zhao, S. *et al.* Improved expression of halorhodopsin for light-induced silencing of neuronal activity. *Brain Cell Biol.* **36,** 141–154 (2008).
9. Gradinaru, V., Thompson, K. R. & Deisseroth, K. eNpHR: a Natronomonas halorhodopsin enhanced for optogenetic applications. *Brain Cell Biol.* **36,** 129–139 (2008).
10. Tateno, M., Ihara, K. & Mukohata, Y. The novel ion pump rhodopsins from *Haloarcula* form a family independent from both the bacteriorhodopsin and archaerhodopsin families/tribes. *Arch. Biochem. Biophys.* **315,** 127–132 (1994).
11. Bamberg, E., Tittor, J. & Oesterhelt, D. Light-driven proton or chloride pumping by halorhodopsin. *Proc. Natl Acad. Sci. USA* **90,** 639–643 (1993).
12. Aravanis, A. M. *et al.* An optical neural interface: *in vivo* control of rodent motor cortex with integrated fiberoptic and optogenetic technology. *J. Neural Eng.* **4,** S143–S156 (2007).
13. Bernstein, J. G. *et al.* Prosthetic systems for therapeutic optical activation and silencing of genetically-targeted neurons. *Proc. Soc. Photo Opt. Instrum. Eng.* **6854,** 68540H (2008).
14. Lin, J. Y., Lin, M. Z., Steinbach, P. & Tsien, R. Y. Characterization of engineered channelrhodopsin variants with improved properties and kinetics. *Biophys. J.* **96,** 1803–1814 (2009).
15. Berthold, P. *et al.* Channelrhodopsin-1 initiates phototaxis and photophobic responses in *Chlamydomonas* by immediate light-induced depolarization. *Plant Cell* **20,** 1665–1677 (2008).
16. Bevensee, M. O., Cummins, T. R., Haddad, G. G., Boron, W. F. & Boyarsky, G. pH regulation in single CA1 neurons acutely isolated from the hippocampi of immature and mature rats. *J. Physiol. (Lond.)* **494,** 315–328 (1996).
17. Chesler, M. Regulation and modulation of pH in the brain. *Physiol. Rev.* **83,** 1183–1221 (2003).
18. Meyer, T. M., Munsch, T. & Pape, H. C. Activity-related changes in intracellular pH in rat thalamic relay neurons. *Neuroreport* **11,** 33–36 (2000).
19. Trapp, S., Luckermann, M., Brooks, P. A. & Ballanyi, K. Acidosis of rat dorsal vagal neurons in situ during spontaneous and evoked activity. *J. Physiol. (Lond.)* **496,** 695–710 (1996).
20. Leinekugel, X. *et al.* Correlated bursts of activity in the neonatal hippocampus *in vivo*. *Science* **296,** 2049–2052 (2002).
21. Wehr, M. & Zador, A. M. Balanced inhibition underlies tuning and sharpens spike timing in auditory cortex. *Nature* **426,** 442–446 (2003).
22. Richter, D. W., Pierrefiche, O., Lalley, P. M. & Polder, H. R. Voltage-clamp analysis of neurons within deep layers of the brain. *J. Neurosci. Methods* **67,** 121–131 (1996).
23. Narikawa, K., Furue, H., Kumamoto, E. & Yoshimura, M. *In vivo* patch-clamp analysis of IPSCs evoked in rat substantia gelatinosa neurons by cutaneous mechanical stimulation. *J. Neurophysiol.* **84,** 2171–2174 (2000).
24. Han, X. *et al.* Millisecond-timescale optical control of neural dynamics in the nonhuman primate brain. *Neuron* **62,** 191–198 (2009).
25. Ming, M. *et al.* pH dependence of light-driven proton pumping by an archaerhodopsin from Tibet: comparison with bacteriorhodopsin. *Biophys. J.* **90,** 3322–3332 (2006).
26. Lukashev, E. P. *et al.* pH dependence of the absorption spectra and photochemical transformations of the archaerhodopsins. *Photochem. Photobiol.* **60,** 69–75 (1994).
27. Lanyi, J. K. Proton transfers in the bacteriorhodopsin photocycle. *Biochim. Biophys. Acta* **1757,** 1012–1018 (2006).
28. Enami, N. *et al.* Crystal structures of archaerhodopsin-1 and -2: common structural motif in archaeal light-driven proton pumps. *J. Mol. Biol.* **358,** 675–685 (2006).
29. Mogi, T., Marti, T. & Khorana, H. G. Structure-function studies on bacteriorhodopsin. IX. Substitutions of tryptophan residues affect protein-retinal interactions in bacteriorhodopsin. *J. Biol. Chem.* **264,** 14197–14201 (1989).
30. Luecke, H., Schobert, B., Richter, H. T., Cartailler, J. P. & Lanyi, J. K. Structure of bacteriorhodopsin at 1.55 Å resolution. *J. Mol. Biol.* **291,** 899–911 (1999).

Supplementary Information is linked to the online version of the paper at www.nature.com/nature.

Acknowledgements E.S.B. acknowledges funding by the NIH Director's New Innovator Award (DP2 OD002002-01), as well as the NSF (0835878 and 0848804), the McGovern Institute Neurotechnology Award Program, the Department of Defense, NARSAD, the Alfred P. Sloan Foundation, Jerry and Marge Burnett, the SFN Research Award for Innovation in Neuroscience, the MIT Media Lab, the Benesse Foundation, and the Wallace H. Coulter Foundation. X.H. acknowledges the Helen Hay Whitney Foundation and NIH 1K99MH085944. The authors thank E. Klinman for help with transfections, R. Desimone for advice, J. Lin for technical aid on intracellular pH measurements, K. Ihara for discussions about archaerhodopsins, and M. Hemann and N. Gershenfeld and the Center for Bits and Atoms for use of their respective laboratory facilities.

Author Contributions B.Y.C., X.H. and E.S.B. designed experiments, analysed data and wrote the paper. B.Y.C. and X.H. carried out experiments. A.S.D. assisted with electrophysiological recording. X.Q., M.L. and A.S.C. assisted with molecular biology, virus making, and transfections. M.A.H. performed Monte Carlo modelling. P.E.M., G.M.B. and Y.L. created hippocampal and cortical neural cultures.

Author Information Sequences are available to download from GenBank (http://www.ncbi.nlm.nih.gov/) under accession numbers: GU045593 (mammalian codon-optimized Arch), GU045594 (mammalian codon-optimized Arch fused to GFP), GU045595 (mammalian codon-optimized Mac), GU045596 (mammalian codon-optimized Mac fused to GFP), GU045597 (ss-Prl-Arch), GU045598 (ss-Arch-GFP-ER2) and GU045599 (ss-Prl-Arch-GFP). Reprints and permissions information is available at www.nature.com/reprints. The authors declare no competing financial interests. Correspondence and requests for materials should be addressed to E.S.B. (esb@media.mit.edu).

SUPPLEMENTARY FIGURES AND LEGENDS

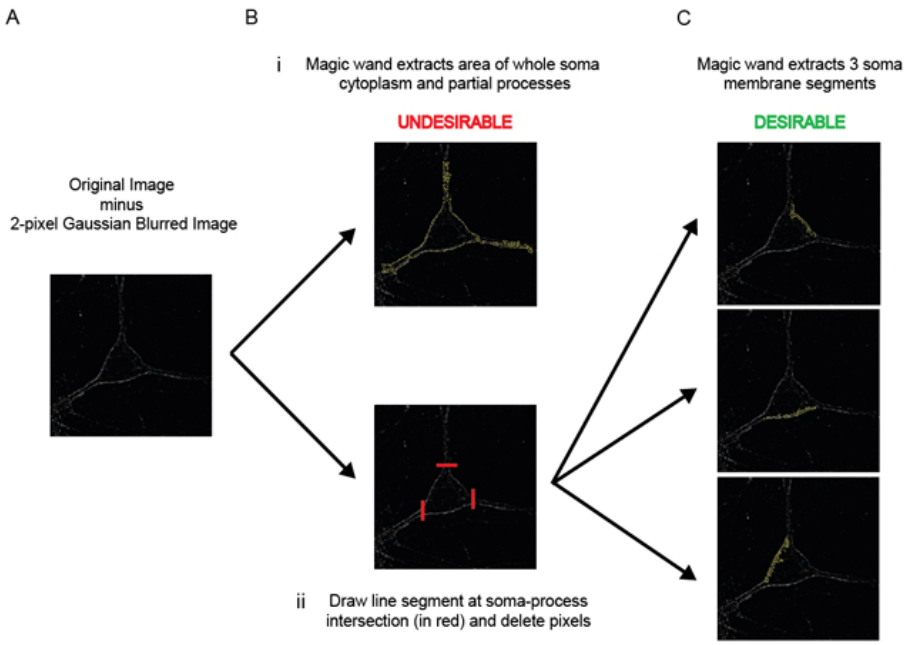

Supplementary Figure 1. Outline of the method used for quantitative analysis of opsin-GFP membrane expression in neurons, modified from ref. [1]. **(A)** The cell contour was first enhanced using the blur and subtraction methodology as described in step C of Supplementary Figure S2 of ref. [1]. **(B)** The Magic Wand tool in ImageJ was used to define the pixels corresponding to the cell membrane. **(i)** However, the tool sometimes selected the whole somatic cytoplasm and the processes, because some neuronal processes were too small to be separated into membrane vs. cytosol, causing the appearance of connectedness, and/or because the well-defined membrane processes overlap with other neurons or extend to the edge of the image. **(ii)** Line sections were generated at the apparent boundary of the soma and its processes, to separate sub-resolution image components from the soma (drawn as red here). **(C)** The Magic Wand tool could now select distinct membrane segments of the soma. Membrane expression

was then quantified by taking the area-weighted average of membrane pixel values, in the original image.

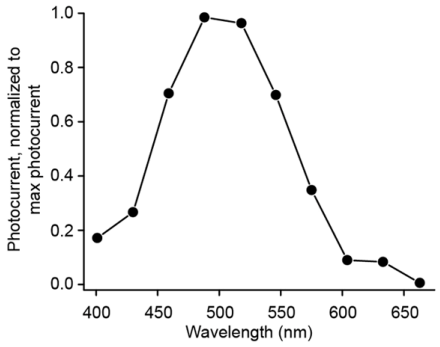

Supplementary Figure 2. The action spectrum of the *Acetabularium acetabulum* proton pump, measured in HEK 293FT cells (N = 5 cells).

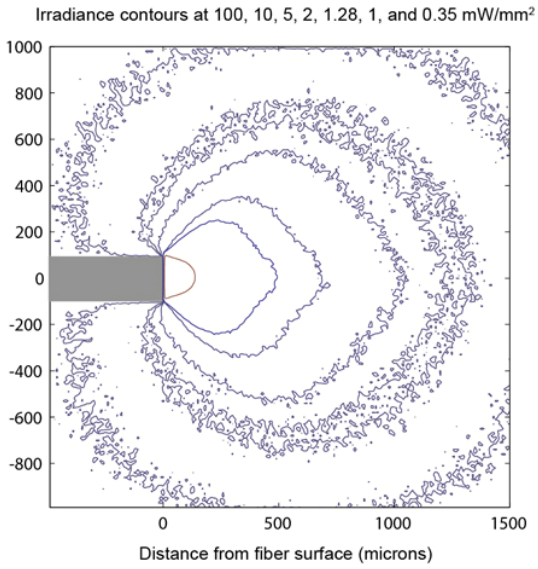

Supplementary Figure 3. 593 nm yellow light irradiance in the brain (gray matter) is plotted as a function of location with respect to the tip of an optical fiber (200 μm in

diameter, represented by the gray rectangle shown at left; the irradiance at the surface of the fiber tip was set at 200 mW/mm^2). Light irradiance was estimated using a Monte Carlo light scattering/absorption simulation. The contours display 100, 10, 5, 2, 1.28, 1, and 0.35 mW/mm^2 irradiances.

SUPPLEMENTARY NOTES

Using the method of **Supplementary Figure 1**, we found that the absolute expression level of Arch on the plasma membrane was similar to that of Halo ($p > 0.2$, N = 5 cells each). We experimented with adding targeting sequences that improve trafficking, and found that adding a signal sequence from the MHC Class I antigen ('ss')[2] as well as the Kir2.1 ER export sequence ('ER2') (which is part of the sequence that boosts Halo currents by 75%, resulting in eNpHR, ref. [3,4]), did not augment Arch currents ($p > 0.6$, N = 16 Arch cells, N = 9 ss-Arch-ER2 cells). Thus, the effect of a given trafficking-improving sequence on opsin expression is opsin-specific (and perhaps species-specific), but nonetheless deserves further attention. For example, adding the Prolactin signal sequence ('Prl')[5] to the N terminus of Arch trended towards boosting the Arch current (+32%; $p < 0.08$, N = 18 ss-Prl-Arch cells). Improving opsin targeting, however, is unlikely to alter opsin recovery kinetics or light dynamic range.

SUPPLEMENTARY TABLES

SUPPLEMENTARY TABLE 1: Molecular screening candidates and references.

Abbreviations	Molecule class	Species of origin	GENBANK Accession	References

Halo, NpHR, pHR	halorhodopsin	*Natronomas pharaonis*	ABQ08589	[6-8]
sHR, HR	halorhodopsin	*Halobacterium salinarum*	NP_279315	[8,9]
aHR-3	archaehalorhodopsin	*Halorubrum sodomense*	BAA75202	[9]
aHR-1, SGHR	archaehalorhodopsin	*Halorubrum aus-1 (sp. SG1)*	CAA49773	[9,10]
cHR-3	cruxhalorhodopsin	*Haloarcula vallismortis*	BAA06679	[11,12]
cHR-5	cruxhalorhodopsin	*Haloarcula marismortui*	AAV46572	[12,13]
SquareHOP	square halorhodopsin	*Haloquadratum walysbyi*	CAJ53165	[14]
dHR-1	deltahalorhodopsin	*Haloterrigena sp. Arg-4*	BAA75201	[9,12]
SalHO, SRU_2780	bacterial halorhodopsin	*Salinibacter ruber*	AAT76430	[15,16]
pop	fungal opsin related protein	*Podospora anserina (DSM980)*	XP_001904282	[17]
nop-1	fungal opsin related protein	*Neospora crassa*	XP_959421	[18]
Mac, LR, Ops	Fungal opsin related protein, bacteriorhodopsin	*Leptosphaeria maculans*	AAG01180	[19]
Arch, aR-3	archaerhodopsin	*Halorubrum*	BAA09452	[9]

		sodomense		
BR	Bacteriorhodopsin	*Halobacterium salinarum*	CAA23744	[9]
cR-1	Cruxrhodopsin	*Haloarcula argentinensis (sp. arg-1*	BAA06678	[20]
gPR, BAC31A8	Proteorhodopsin	*γ - proteobacterium BAC31A8*	AAG10475	[21,22]
bPR, Hot75m4	proteorhodopsin	*γ- proteobacterium Hot75m4*	Q9AFF7	[21,22]
Ace, AR	Algal bacteriorhodopsin	*Acetabularia acetabulum*	AAY82897	[23]

Summary of molecules screened, including abbreviations, molecule classification, species of origin, GenBank accession number, and references. Major molecule types are defined as "bacteriorhodopsins" or "rhodopsins" for outwardly rectifying proton pumps and "halorhodopsins" for inwardly rectifying chloride pumps. Sub-classifications of molecule type are determined by kingdom and/or genus of species of origin (e.g. archaerhodopsin = proton pump from halorubrum genus of halobacteria / haloarchaea).

SUPPLEMENTARY TABLE 2: Action spectra of screened candidates.

Abbreviations	Molecule class	Species of origin	GENBANK Accession	Primary Peak ± FWHM (nm), second order Gaussian fit	Spectral Screen Normalization Factor, relative to Halo (see Experimental Procedures)
Halo, NpHR, pHR	halorhodopsin	*Natronomas pharaonis*	ABQ08589	586 ± 52	1
sHR, HR	halorhodopsin	*Halobacterium salinarum*	NP_279315	No measured photocurrent	N/A

aHR-3	archaehalorhodopsin	*Halorubrum sodomense*	BAA75202	586 ± 63	1.18
aHR-1, SGHR	archaehalorhodopsin	*Halorubrum aus-1 (sp. SG1)*	CAA49773	No measured photocurrent	N/A
cHR-3	cruxhalorhodopsin	*Haloarcula vallismortis*	BAA06679	592 ± 58	1.17
cHR-5	cruxhalorhodopsin	*Haloarcula marismortui*	AAV46572	594 ± 52	1.10
SquareHOP	square halorhodopsin	*Haloquadratum walysbyi*	CAJ53165	[1443271919]No measured photocurrent	N/A
dHR-1	deltahalorhodopsin	*Haloterrigena sp. Arg-4*	BAA75201	No measured photocurrent	N/A
SalHO, SRU_2780	bacterial halorhodopsin	*Salinibacter ruber*	AAT76430	582 ± 71	1.12
Pop	fungal opsin related protein	*Podospora anserina (DSM980)*	XP_001904282	No measured photocurrent	N/A
nop-1	fungal opsin related protein	*Neospora crassa*	XP_959421	No measured photocurrent	N/A
Mac, LR, Ops	fungal opsin related protein, bacteriorhodopsin	*Leptosphaeria maculans*	AAG01180	550 ± 69	0.94
Arch, aR-3	archaerhodopsin	*Halorubrum sodomense*	BAA09452	566 ± 66	1.08
BR	bacteriorhodopsin	*Halobacterium salinarum*	CAA23744	572 ± 75	1.26
cR-1	cruxrhodopsin	*Haloarcula argentinensis*	*BAA06678*	557 ± 67	1.23
gPR, BAC31A8	proteorhodopsin	*γ-proteobacterium BAC31A8*	AAG10475	No measured photocurrent	N/A
bPR, Hot75m4	proteorhodopsin	*γ-proteobacterium Hot75m4*	Q9AFF7	No measured photocurrent	N/A
Ace, AR	algal bacteriorhodopsin	*Acetabularia acetabulum*	AAY82897	505 ± 57	0.98

Reported peaks and full-width at half-maximum values are from second order Gaussian fits, in order to account for the characteristic “shoulder” of rhodopsins. “Spectral Screen Normalization Factor” accounts for differences in measured photocurrents due to varying excitation efficiencies via use of limited bandpass illumination filters (575 ± 25 nm, 535 ± 25 nm) for all molecules in the screen (see **Supplementary Methods** for normalization protocol). All data reported was measured in neurons, except for Ace (*Acetabularia acetabulum* bacteriorhodopsin homolog), which was measured in HEK 293FT cells (**Supplementary Figure 2**), in order to obtain a precise spectrum given the very low currents observed in neurons.

SUPPLEMENTARY TABLE 3: Action spectrum and spontaneous recovery to active pumping state in the dark for *N. pharaonis* halorhodopsin (Halo, NpHR) point mutants examined in HEK293FT cells.

Halo point mutant	Homologous *H. salinarum* HR residue	Homologous *H. salinarum* BR residue	Primary predicted outcome of mutation	Primary Peak ± FWHM (nm), second order Gaussian fit	Recovery of active pumping in dark?
Wild type	N/A	N/A	N/A	584 ± 51	No
T126H	T111	D85	Recovery	No measured photocurrent	No
T126R	T111	D85	Recovery	No measured photocurrent	No
W127F	W112	W86	Spectral shift	No measured photocurrent	No
S130T	S130	T89	Recovery	568 ± 55	No
S130D	S130	T89	Recovery	No measured photocurrent	No
S130H	S130	T89	Recovery	No measured photocurrent	No
S130R	S130	T89	Recovery	No measured photocurrent	No
A137T	A122	D96	Recovery	585 ± 52	No
A137D	A122	D96	Recovery	575 ± 53	No
A137H	A122	D96	Recovery	No measured photocurrent	No
A137R	A122	D96	Recovery	No measured photocurrent	No
G163C	G148	G122	Spectral shift	No measured photocurrent	No
W179F	W164	W137	Spectral shift	No measured photocurrent	No
S183C	F168	S141	Spectral shift	No measured photocurrent	No
F187M	F172	M145	Spectral shift	589 ± 52	No
F187A	F172	M145	Spectral shift	No measured photocurrent	No
K215H	R200	R149	Recovery	586 ± 50	No
K215R	R200	R149	Recovery	575 ± 51	No
K215Q	R200	R149	Recovery	585 ± 56	No
T218S	T203	T178	Recovery	582 ± 53	No
T218D	T203	T178	Recovery	No measured photocurrent	No
T218H	T203	T178	Recovery	No measured photocurrent	No
T218R	T203	T178	Recovery	No measured photocurrent	No
W222F	W207	W182	Spectral shift	No measured photocurrent	No
P226V	P211	P186	Spectral shift	No measured	No

				photocurrent	
P226G	P211	P186	Spectral shift	No measured photocurrent	No
W229F	W214	W189	Spectral shift	587 ± 53	No

Reported peaks and full-width at half-maximum values are from second order Gaussian fits, in order to account for the characteristic "shoulder" of rhodopsins. The column "Primary predicted outcome of mutation" lists hypothesized outcomes as to what parameters of molecular performance might be expected to change, for each mutation. The term "Recovery" refers to spontaneous recovery of the active pumping state in the dark over a timescale of seconds, which holds for Arch and ChR2 but not for Halo (i.e. see **Figure 1D-E** in main text and also ref. [24]). "Recovery" candidate residues were targeted based on their hypothesized roles in chloride affinities and/or transport kinetics, as determined by structure-function studies and mutation studies using other halorhodopsins[25-28]. Spectral residues were targeted based on their predicted retinal flanking locations based on crystal structures, and/or have been shown previously to govern the spectrum of bacteriorhodopsin[29-34]. Alignments to *H. salinarum* halorhodopsin and bacteriorhodopsins were made using NCBI Blast.

SUPPLEMENTARY METHODS

Novel opsin reagents: plasmid construction and lentivirus production.

The opsins examined in this study are listed in **Supplementary Table 1**, which describes their molecule classes, species of origin, GenBank Accession numbers, and relevant references. Molecule classes chiefly include bacteriorhodopsins (proton pumps) and halorhodopsins (chloride pumps). Further sub-classifications of ion pump type denote the origin of the species: for example, a "cruxhalorhodopsin" is a chloride pump from the *haloarcula* genus of halobacteria.

Opsins were mammalian codon-optimized, and were synthesized by Genscript (Genscript Corp., NJ). Opsins were fused in frame, without stop codons, ahead of GFP (using BamHI and AgeI) in a lentiviral vector containing the CaMKII promoter[35], enabling direct neuron transfection, HEK cell transfection (expression in HEK cells is enabled by a ubiquitous promoter upstream of the lentiviral cassette), and lentivirus production (except for *Halobacterium salinarum* halorhodopsin, which was fused to GFP in the vector pEGFP-N3 (using EcoRI and BamHI) and only tested by transfection). eNpHR was synthesized as described before[4], by inserting the signaling sequence from the acetycholine receptor beta subunit (amino acid sequence: MRGTPLLLVVSLFSLLQD; DNA sequence: atgaggggtacgcccctgctcctcgtcgtctctctgttctctctgcttcaggac) at the N-terminus, and the ER2 sequence (amino acid sequence: FCYENEV; DNA sequence: ttctgctacgagaatgaagtg) at the C-terminus of Halo[36,37]. The 'ss' signal sequence from truncated MHC class I antigen corresponded to amino acid sequence (M)VPCTLLLLLAAALAPTQTRA, DNA sequence GTCCCGTGCACGCTGCTCCTGCTGTTGGCAGCCGCCCTGGCTCCGACTCAGACGCGGGC C[2]. The 'Prl' Prolactin signal sequence corresponded to amino acid sequence MDSKGSSQKGSRLLLLLVVSNLLLCQVVS, DNA sequence gacagcaaaggttcgtcgcagaaagggtcccgcctgctcctgctgctggtggtgtcaaatctactcttgtgccagggtgtggtctccacc cccgtc[5,38]. Halo point mutants for HEK cell testing were generated using the QuikChange kit (Stratagene) on the Halo-GFP fusion gene inserted between BamHI and EcoRI sites in the pcDNA 3.1 backbone (Invitrogen). All constructs were verified by sequencing, and codon-optimized sequences of key opsins were submitted to Genbank (mammalian codon-optimized Arch, GU045593; mammalian codon-optimized Arch fused to GFP, GU045594; mammalian codon-optimized Mac, GU045595; mammalian codon-optimized Mac fused to GFP, GU045596;

ss-Prl-Arch, GU045597; ss-Arch-GFP-ER2, GU045598; ss-Prl-Arch-GFP, GU045599) and made available for request at:

http://syntheticneurobiology.org/protocols

The amino acid sequence of Arch is:

MDPIALQAGYDLLGDGRPETLWLGIGTLLMLIGTFYFLVRGWGVTDKDAREYYAVTILVPGIASA
AYLSMFFGIGLTEVTVGGEMLDIYYARYADWLFTTPLLLLDLALLAKVDRVTIGTLVGVDALMIVT
GLIGALSHTAIARYSWWLFSTICMIVVLYFLATSLRSAAKERGPEVASTFNTLTALVLVLWTAYPI
LWIIGTEGAGVVGLGIETLLFMVLDVTAKVGFGFILLRSRAILGDTEAPEPSAGADVSAAD.

The amino acid sequence for Mac is:

MIVDQFEEVLMKTSQLFPLPTATQSAQPTHVAPVPTVLPDTPIYETVGDSGSKTLWVVFVLMLIA
SAAFTALSWKIPVNRRLYHVITTIITLTAALSYFAMATGHGVALNKIVIRTQHDHVPDTYETVYRQ
VYYARYIDWAITTPLLLLDLGLLAGMSGAHIFMAIVADLIMVLTGLFAAFGSEGTPQKWGWYTIA
CIAYIFVVWHLVLNGGANARVKGEKLRSFFVAIGAYTLILWTAYPIVWGLADGARKIGVDGEIIAY
AVLDVLAKGVFGAWLLVTHANLRESDVELNGFWANGLNREGAIRIGEDDGA.

Replication-incompetent VSVg-pseudotyped lentivirus was produced as previously described[39], which allows the preparation of clean, non-toxic, high-titer virus (roughly estimated at ~10^9-10^{10} infectious units/mL). Briefly, HEK293FT cells (Invitrogen) were transfected with the lentiviral plasmid, the viral helper plasmid pΔ8.74, and the pseudotyping plasmid pMD2.G. The supernatant of transfected HEK cells containing virus was then collected 48 hours after

transfection, purified, and then pelletted through ultracentrifugation. Lentivirus pellet was resuspended in phosphate buffered saline (PBS) and stored at −80°C until further usage *in vitro* or *in vivo*.

Hippocampal and cortical neuron culture preparation, transfection, infection, and imaging.

All procedures involving animals were in accordance with the National Institutes of Health Guide for the care and use of laboratory animals and approved by the Massachusetts Institute of Technology Animal Care and Use Committee. Swiss Webster or C57 mice (Taconic or Jackson Labs) were used. For hippocampal cultures, hippocampal regions of postnatal day 0 or day 1 mice were isolated and digested with trypsin (1 mg/ml) for ~12 min, and then treated with Hanks solution supplemented with 10-20% fetal bovine serum and trypsin inhibitor (Sigma). Tissue was then mechanically dissociated with Pasteur pipettes, and centrifuged at 1000 rpm at 4°C for 10 min. Dissociated neurons were plated at a density of approximately four hippocampi per 20 glass coverslips, coated with Matrigel (BD Biosciences). For cortical cultures, dissociated mouse cortical neurons (postnatal day 0 or 1) were prepared as previously described[40], and plated at a density of 100-200k per glass coverslip coated with Matrigel (BD Biosciences). Cultures were maintained in Neurobasal Medium supplemented with B27 (Invitrogen) and glutamine. Hippocampal and cortical cultures were used interchangeably; no differences in reagent performance were noted.

Neurons were transfected at 3-5 days *in vitro* using calcium phosphate (Invitrogen). GFP fluorescence was used to identify successfully transfected neurons. Alternatively, neurons were infected with 0.1-1 μl of lentivirus per well at 3-5 days *in vitro*. Throughout the paper, neurons

were transfected unless indicated as having been infected. All images and electrophysiological recordings were made on neurons 9–14 days *in vitro* (approximately 6–10 days after transfection or viral infection).

Confocal images of infected neurons in culture (briefly fixed in 4% paraformaldehyde) were obtained with a Zeiss LSM 510 confocal microscope (63X magnification objective lens). Culture images were maximum intensity projections made from sets of 5 images (1.0 μm image plane thickness) spaced along the z-axis by 0.5 micron steps. Quantitative confocal analysis of membrane expression of opsins was performed using infected neurons in culture (10 days post-infection, briefly fixed in 4% paraformaldehyde). Images were obtained with a Zeiss LSM 510 confocal microscope (63X magnification objective lens), always with the same illumination and observation parameters to avoid procedural variability. Given the near-100% viral infection rate, isolated neurons were chosen for analysis in order to reduce background fluorescence from nearby neurons and their processes. Images were analyzed in ImageJ (National Institutes of Health), based on a neuron-adapted version of a previously reported algorithm[1] used to assay membrane expression of channelrhodopsins and channelrhodopsin variants in HEK cells. An image was first filtered with a 2-pixel Gaussian blur, and the filtered image was subtracted from the original one to enhance the contour of the cell. (These steps are exactly the same as those utilized before in HEK cells[1]; an example of the mathematically enhanced contour is shown in **Supplementary Figure 1A**.) However, because the membranes of neurons do not form simple shapes like the HEK cells as the original algorithm was designed for (**Supplementary Figure 1Bi**), we applied black line sections to separate the neuronal cell body from the processes, as demonstrated in **Supplementary Figure 1Bii** (where the line is in red to aid the eye for these pictures). The magic wand can then accurately select the somatic membrane segments of a neuron (see **Supplementary Figure 1C**), which can then be analyzed by the pixel intensity-

value extraction method described for HEK cells in ref. [1]. The value of the membrane fluorescence for a given neuron, reported in the text, was then defined as the area-weighted average of the line segments. While this method cannot prove that a given patch of membrane-proximal fluorescence exists exclusively on the outermost membrane (in principle a patch of fluorescence could reside just under the membrane), it does serve to discriminate between surface expression and ER retention, and has previously been validated in predicting functional physiological surface expression[1].

***In vitro* patch clamp recording and optical methods**.

Whole cell patch clamp recordings were made on neurons at 9-14 days *in vitro*, using a Multiclamp 700B amplifier, Digidata 1440 digitizer, and a PC running pClamp (Molecular Devices). During recording, neurons were bathed in Tyrode solution containing (in mM): 125 NaCl, 2 KCl, 3 $CaCl_2$, 1 $MgCl_2$, 10 HEPES, 30 glucose, 0.01 NBQX, and 0.01 gabazine, at pH 7.3 (NaOH adjusted), and with 305-310 mOsm (sucrose adjusted). Borosilicate glass (Warner) pipettes were filled with a solution containing (in mM): 125 K-Gluconate, 8 NaCl, 0.1 $CaCl_2$, 0.6 $MgCl_2$, 1 EGTA, 10 HEPES, 4 Mg-ATP, 0.4 Na-GTP, at pH 7.3 (KOH adjusted), and with 295-300 mOsm (sucrose adjusted). Pipette resistance was 5-10 MΩ; access resistance was 10–30 MΩ, monitored throughout the voltage-clamp recording; resting membrane potential was ~ -60 mV in current-clamp recording.

For ion selectivity tests (**Fig. 2A**), neurons were bathed in chloride-free recording solution containing (in mM): 125 Na-Gluconate, 2 K-Gluconate, 3 $CaSO_4$, 1 $MgSO_4$, 10 HEPES, 30 glucose, 0.01 NBQX, 0.01 gabazine, at pH 7.3 (NaOH adjusted), and with 305-310 mOsm (sucrose adjusted), or potassium-free recording solution containing (in mM): 125 NaCl, 2 CsCl,

3 $CaCl_2$, 1 $MgCl_2$, 10 HEPES, 30 glucose, 0.01 NBQX, 0.01 gabazine, at pH 7.3 (NaOH adjusted), 305-310 mOsm (sucrose adjusted). During these ion selectivity tests, pipettes were filled with chloride-free pipette solution containing (in mM): 125 K-Gluconate, 8 Na-Gluconate, 0.1 $CaSO_4$, 0.6 $MgSO_4$, 1 EGTA, 10 HEPES, 4 Mg-ATP, 0.4 Na-GTP, pH 7.3 (KOH adjusted), 295-300 mOsm (sucrose adjusted), or potassium-free pipette solution containing (in mM): 125 Cs-methanesulfonate, 8 Na-Gluconate, 0.1 $CaSO_4$, 0.6 $MgSO_4$, 1 EGTA, 10 HEPES, 4 Mg-ATP, 0.4 Na-GTP, pH 7.3 (CsOH adjusted), 295-300 mOsm (sucrose adjusted). During resting membrane potential shifting (**Fig. 2B**), neurons were bathed in recording solution containing (in mM): 125 N-methyl-D-glucamine, 2 Cs-methanesulfonate, 3 $CdSO_4$, 1 $MgSO_4$, 10 HEPES, 30 glucose, 0.01 NBQX, 0.01 gabazine, pH 7.3 (H_2SO_4 adjusted), 305-310 mOsm (sucrose adjusted), and pipettes were also filled with analogous solutions containing (in mM): 125 Cs-methanesulfonate, 8 N-methyl-D-glucamine, 0.1 $CdSO_4$, 0.6 $MgSO_4$, 1 EGTA, 10 HEPES, 4 Mg-ATP, 0.4 Tris-GTP, pH 7.3 (CsOH adjusted), 295-300 mOsm (sucrose adjusted).

Photocurrents were measured with 1-second or 15-second duration light pulses in neurons voltage clamped at -60mV. Light-induced membrane hyperpolarizations were measured with 1-second light pulses, in neurons current clamped at their resting membrane potential. For all experiments except for the action spectrum characterization experiments, a DG-4 optical switch with 300 W xenon lamp (Sutter Instruments) was used to deliver light pulses. The DG-4 was controlled via TTL pulses generated through a Digidata signal generator. A 575 ± 25 nm bandpass filter (Chroma) was used to deliver yellow light, and a 535 ± 25 nm filter was used to deliver green light. For selective activation of Halo versus Mac at different wavelengths (**Fig. 4**), a 470 ± 20 nm bandpass filter (Chroma) was used to deliver blue light (0.92 mW/mm^2, through a 40x objective), and a 630 ± 15 (Chroma) was used to deliver red light (2.6 mW/mm^2). For action

spectrum characterization (**Fig. 1B**, **Fig. 4A**, **Supplementary Table 2**), a Till Photonics PolyChrome V, 150 W Xenon, 15nm monochromator bandwidth, was used.

Data was analyzed using Clampfit (Molecular Devices) and MATLAB (Mathworks, Inc.). Statistical analysis and curve fitting was done with Statview (SAS Institute), MATLAB, or Origin (OriginLab). Reported action spectra are second-order Gaussian fits (performed in MATLAB), because action spectra were asymmetric, with a broad "shoulder" at wavelengths shorter than the primary peak wavelength.

For the initial screening of photocurrents (**Fig. 1A**), yellow light (575 $\pm$ 25 nm, 7.8 mW/mm^2, through a 40x lens) was chiefly used (see below for exceptions); accordingly, in order to adjust the screen data to reflect the photocurrent for each molecule that would have been observed at its respective spectral maximum, photocurrents were spectrum normalized by calculating the overlap integral between the second-order Gaussian fit of the action spectrum for each molecule and the passband of the yellow illumination filter used for the screen (or in other words, integrating the Gaussian fit between 550 and 600 nm), and then dividing that value by the integral of the whole action spectrum for that molecule. These resultant ratios, or "Spectral Screen Normalization Factors," are summarized (normalized to that ratio for Halo itself) in the rightmost column of **Supplementary Table 2**. In the cases of gPR, bPR, and the *Leptosphaeria maculans* (Mac, LR, Ops) and *Acetabularia acetabulum* (Ace, AR) proton pump opsins, green light (535 ± 25 nm, 9.4 mW/mm^2, through a 40x lens) was used during the screen, due to the significantly blue-shifted action spectrum of these genes. These four spectra were also normalized to the respective spectral maxima of each molecule, as described above, as well as weighted by the output power of the lamp. All screen photocurrents and spectra (**Fig.**

1A, Fig. 1B, Fig. 4A, Supplementary Table 2) were measured in neurons except for the action spectrum of Ace (**Supplementary Figure 2**), which was recorded in HEK 293FT cells for better resolution (due to the extremely small currents of Ace in neurons, **Fig. 1A**).

In order to extend our power characterization of Arch beyond the power of the yellow light available on our microscope using the configuration that we utilized (7.8 mW/mm^2 irradiance, through a 40x lens), we extrapolated to higher effective yellow powers by equating various powers of unfiltered white light illumination from the DG4, to approximate effective yellow power equivalents (**Fig. 1Fii**). These effective irradiances were estimated by adjusting the output power of unfiltered white light from the DG4, and comparing the photocurrents vs. those generated with 575 ± 25 nm yellow light in the same Arch-expressing neuron, at low light powers, until the photocurrent magnitudes were similar ($p > 0.7$, paired t-test; N = 6). In support of this method for estimating effective irradiances, we did not observe noticeable photocycle-accelerating effects of non-yellow light for Arch. Light power-photocurrent curves, thus estimated, were fitted with a Hill plot (**Fig. 1F**). To compare to Arch, Halo currents measured for the dose response experiment (**Fig. 1F**) were obtained using a Halo variant that demonstrated similar photocurrent densities compared to unmodified Halo ($p > 0.7$, t-test; N = 16), bearing a N-terminal signal sequence from a truncated MHC class I antigen (VPCTLLLLLAAALAPTQTRA, see above) and the C-terminal golgi export sequence from bovine rhodopsin (TETSQVAPA); these measurements were then scaled by the photocurrent ratio between Halo and this variant measured at 7.8 mW/mm^2, to yield the curve shown in **Fig. 1F**.

HEK cell culture, transfection, and electrophysiology.

HEK 293FT cells (Invitrogen) were maintained in DMEM medium (Cellgro) supplemented with 10% fetal bovine serum (Invitrogen), 1% penicillin/streptomycin (Cellgro) and 1% sodium pyruvate (Biowhittaker)). For recording, cells were plated at 5-10% confluence on uncoated glass coverslips, where they adhered to surfaces typically within 12-18 hours. Adherent cells were transfected using TransIT 293 transfection kits (Mirus). Cells were recorded by whole-cell patch clamp 1.5 – 2 days later, as described above for neurons, except that they were voltage clamped at -40 mV, with a Tyrode bath solution lacking GABAzine and NBQX.

Intracellular pH imaging.

Intracellular pH (denoted pH_i) imaging was performed using a cell-permeant ratiometric fluorescent dye, carboxy-SNARF-1 AM ester (Invitrogen), based on previously reported methods[41,42]. In order to eliminate background fluorescence that would interfere with pH_i imaging using SNARF-1, we utilized the fusion protein comprising Arch and cyan fluorescent protein (CFP). The DG-4 was used to deliver light pulses (6.1 mW/mm^2, through a 20x lens) via a green 535 ± 25 nm bandpass filter (Chroma). Neurons were loaded with 10 μM SNARF-1-AM ester in Tyrode solution for 10 minutes, and then washed twice with Tyrode. Arch-expressing neurons were identified by their CFP fluorescence (Chroma CFP set, $\lambda_{excitation}$ = 436 ± 20 nm, $\lambda_{dicrhoic}$ = 455 nm, $\lambda_{emission}$= 480 ± 20 nm). After waiting 1 additional minute, Arch and the SNARF-1 dye were simultaneously excited with 535 ± 25 nm light, and the dye was imaged near the isosbestic point of the dye for 500 ms using a 610 ± 37.5 nm bandpass filter ($\lambda_{dichroic}$ = 565 nm, Chroma) to obtain a baseline SNARF loading level. After waiting another minute for the neuron to recover its initial pH_i, the neuron and dye were again excited with green light, and the dye was imaged at various time points with 1 second exposure lengths, using a 640 ± 25 nm bandpass filter ($\lambda_{dichroic}$ = 600 nm, Chroma). Arch-negative neighboring neurons in the same

field of view were imaged to provide a basis for comparison, and also to provide baseline pH of the cells as a point of reference, as done in ref. [41]. Immediately after this period, the dye was again imaged near the isobestic point for 500 ms to assess for photo-bleaching or dye leakage; no change was observed ($p > 0.7$ comparing before vs. after 60 seconds of illumination; $n = 5$ neurons).

Calibration of the dye was performed by the "high K^+/nigericin" method[42], in which cells were immersed in a high K^+ Tyrode-like solution containing (in mM): 125 KCl, 2 NaCl, 3 $CaCl_2$, 1 $MgCl_2$, 10 HEPES, 30 glucose, 0.01 NBQX, 0.01 gabazine, 0.001 TTX, pH 5.5 and pH 8.5 initial stock solutions (KOH adjusted), 305-310 mOsm (sucrose adjusted). The calibration curve was taken between pH 6.75 and 8 (N = 51 – 110 neurons per calibration point; calibration curve linear region goodness of fit $R^2 = 0.999$, between pH 7.15 – 8.0). Images were processed using ImageJ (National Institutes of Health).

Cell health assays.

Membrane properties were measured on day 11 *in vitro* (**Fig. 2E-2G**) using algorithms built into pClamp10. Cell death (**Fig. 2D**) was assayed at day 18 *in vitro* by incubating cultured neurons for 10 minutes in 0.04% Trypan Blue (Gibco) in Tyrode solution for 10 minutes at room temperature, washing with Tyrode solution, and then immediately counting the percentage of neurons stained. In order to limit variability across cell cultures and cell ages, Arch and wild type control neurons were chosen from the same cell cultures and tested on the same day.

Estimations of thresholds for silencing.

To acquire the data in **Fig. 3A**, whole-cell current-clamped neurons were somatically injected with 5Hz current pulse trains (15 ms pulse duration, 8 sec train duration) at 200, 350, or 500 pA, with or without yellow light (575 nm) illumination at irradiances of 6, 1.28, or 0.35 mW/mm^2 for 3 seconds, beginning 2 seconds into the current pulse train. Neurons that did not spike at all with 200 pA current pulses (15 ms pulse duration) were discarded. For all remaining cells, the probability of spiking in the dark, given a 200 pA/15 ms current input, was 84.0 ± 10.5% and 82.8 ± 3.5% for Halo- and Arch-expressing neurons, respectively ($p > 0.9$, N =7-8 neurons each), and the probability of spiking in the dark was ~100%, given ≥ 350 pA current inputs.

Virus injection.

Under isoflurane anesthesia, 1 μL lentivirus was injected through a craniotomy made in the mouse skull, into the motor cortex (0.62 mm anterior, 0.5 mm lateral, and 0.5 mm deep, relative to bregma), or the sensory cortex (0.02 mm posterior, 3.2 mm lateral, and 2.2 mm deep, relative to bregma). Virus was injected at a rate of 0.1-0.2 μl/min through a cannula connected via polyethylene tubing to a Hamilton syringe, placed in a syringe pump (Harvard Apparatus). The syringe, tubing, and cannula were filled with silicone oil (Sigma). For mice used for *in vivo* recordings, custom-fabricated plastic headplates were affixed to the skull[43], and the craniotomy was protected with agar and dental acrylic.

***In vivo* physiology, optical neuromodulation, and data analysis.**

Recordings were made in the cortex of headfixed awake mice 1-2 months after virus injection, using glass microelectrodes of 5-20 MΩ impedance filled with PBS, containing silver/silver-chloride wire electrodes. Signals were amplified with a Multiclamp 700B amplifier and digitized

with a Digidata 1440, using pClamp software (Molecular Devices). A 50 mW yellow laser (SDL-593-050T, Shanghai Dream Laser) was coupled to a 200 micron-diameter optical fiber in a fashion as described previously[39,44]. The laser was controlled via TTL pulses generated through Digidata. Laser light power was measured with an 818-SL photodetector (Newport Co.). An optical fiber was attached to the recording glass electrode, with the tip of the fiber ~600 μm laterally away from and ~500 μm above the tip of the electrode (e.g., ~800 microns from the tip), and guided into the brain with a Siskiyou manipulator at a slow rate of ~1.5 μm/s to minimize deformation of the cortical surface.

Data was analyzed using MATLAB (Mathworks, Inc.). Spikes were detected and sorted offline using Wave_clus (http://vis.caltech.edu/~rodri/Wave_clus/Wave_clus_home.htm). Neurons suppressed during light were identified by performing a paired t-test, for each neuron, between the baseline firing rate during the 5 second period before light onset vs. during the period of 5 second light illumination, across all trials for that neuron, thresholding at the $p < 0.05$ significance level, as previously described[39]. Instantaneous firing rate histograms were computed by averaging the instantaneous firing rate for each neuron, across all trials, with a histogram time bin of 20 ms duration. To determine the latency between light onset and the neural response, we swept a 20 ms-long sliding window through the electrophysiology data and looked for the earliest 20 ms period that deviated from baseline firing rate, as assessed by performing a paired t-test for the firing rate during each window vs. during the baseline period, across all trials for each neuron. Latency was defined as the time from light onset to the time at which firing rate was significantly different from baseline for the following 120 ms. The time for after-light suppression to recover back to baseline was calculated similarly.

Histology.

Between 2 and 8 weeks after virus injection, mice were perfused through the left cardiac ventricle with ~20 mL 4% paraformaldehyde in PBS (pH 7.3), and then the brain was removed and sectioned into 120-240 μm coronal sections on a vibratome in ice-cold PBS, and stored in PBS. Slices were mounted with Vectashield solution (Vector Labs), and visualized with a Zeiss LSM 510 confocal microscope using 20x and 63x objective lenses.

Monte Carlo modeling of light propagation.

In MATLAB, we performed Monte Carlo simulation of light scattering and absorption in the brain from light emitted from the end of an optical fiber by dividing a cube of gray matter into a 200 x 200 x 200 grid of voxels corresponding to 10 μm x 10 μm x 10 μm in dimension, using previously-published model parameters and algorithms[45-47]. We interpolated data from ref. [45] to obtain a scattering coefficient for yellow (~593 nm) light in brain gray matter of 13 mm^{-1}, and an absorption coefficient of 0.028 mm^{-1}. Since we were interested in light propagation close to the optical fiber, before the orientation of photon trajectories is randomized by multiple scattering events, we used an anisotropic scattering model based upon the Henyey-Greenstein phase function, utilizing an anisotropy parameter of 0.89[45,46]. We launched 5 x 10^6 packets of photons in a fiberlike radiation pattern through a model fiber (Optran 0.48 HPCS, Thorlabs) with a numerical aperture of 0.48, and modeled their propagation into the brain based on the algorithm of ref. [47]. In essence, whenever a photon packet entered a voxel, our program would probabilistically calculate the forecasted traveling distance before the next scattering event. If that traveling distance took the photon packet out of the starting voxel, then the packet would be partially absorbed appropriately for the distance it traveled within the starting voxel, and the process would then restart upon entry of the photon packet into the new voxel. If that traveling

distance ended the trip of the photon packet within the starting voxel, then the packet would be absorbed appropriately for the distance it traveled within the starting voxel, and a new direction of packet propagation would be randomly chosen according to the Henyey-Greenstein function. Using this model, we generated **Supplementary Figure 3,** which shows the contours at which the light irradiance falls off to various percentages of the irradiance of light at the surface of the optical fiber, for yellow light. The model generally agrees with previous measurements, done in brain slices[48].

SUPPLEMENTARY REFERENCES

1 Wang, H. *et al.* Molecular determinants differentiating photocurrent properties of two channelrhodopsins from chlamydomonas. *J Biol Chem* **284**, 5685-5696 (2009).

2 Munoz-Jordan, J. L. *et al.* Inhibition of alpha/beta interferon signaling by the NS4B protein of flaviviruses. *J Virol* **79**, 8004-8013 (2005).

3 Zhao, S. *et al.* Improved expression of halorhodopsin for light-induced silencing of neuronal activity. *Brain cell biology* **36**, 141-154 (2008).

4 Gradinaru, V., Thompson, K. R. & Deisseroth, K. eNpHR: a Natronomonas halorhodopsin enhanced for optogenetic applications. *Brain cell biology* **36**, 129-139 (2008).

5 Jungnickel, B. & Rapoport, T. A. A posttargeting signal sequence recognition event in the endoplasmic reticulum membrane. *Cell* **82**, 261-270 (1995).

6 Han, X. & Boyden, E. S. Multiple-color optical activation, silencing, and desynchronization of neural activity, with single-spike temporal resolution. *PLoS ONE* **2**, e299 (2007).

7 Zhang, F. *et al.* Multimodal fast optical interrogation of neural circuitry. *Nature* **446**, 633-639 (2007).

8 Váró, G. Analogies between halorhodopsin and bacteriorhodopsin. *Biochimica et Biophysica Acta (BBA) - Bioenergetics* **1460**, 220-229 (2000).

9 Mukohata, Y., Ihara, K., Tamura, T. & Sugiyama, Y. Halobacterial rhodopsins. *J Biochem* **125**, 649-657 (1999).

10 Soppa, J., Duschl, J. & Oesterhelt, D. Bacterioopsin, haloopsin, and sensory opsin I of the halobacterial isolate Halobacterium sp. strain SG1: three new members of a growing family. *J Bacteriol* **175**, 2720-2726 (1993).

11 Kitajima, T. *et al.* Novel bacterial rhodopsins from Haloarcula vallismortis. *Biochem Biophys Res Commun* **220**, 341-345 (1996).

12 Klare, J. P., Chizhov, I. & Engelhard, M. Microbial rhodopsins: scaffolds for ion pumps, channels, and sensors. *Results Probl Cell Differ* **45**, 73-122 (2008).

13 Baliga, N. S. *et al.* Genome sequence of Haloarcula marismortui: a halophilic archaeon from the Dead Sea. *Genome Res* **14**, 2221-2234 (2004).

14 Bolhuis, H. *et al.* The genome of the square archaeon Haloquadratum walsbyi : life at the limits of water activity. *BMC Genomics* **7**, 169 (2006).

15 Mongodin, E. F. *et al.* The genome of Salinibacter ruber: convergence and gene exchange among hyperhalophilic bacteria and archaea. *Proc Natl Acad Sci U S A* **102**, 18147-18152 (2005).

16 Antón, J. *et al.* in *Adaptation to Life in High Salt Concentrations in Archaea, Bacteria and Eukarya* eds N. Gunde-Cimerman, Plemenitas. A, & A. Oren) 257–266. (Kluwer Academic Publishers, 2005).

17 Espagne, E. *et al.* The genome sequence of the model ascomycete fungus Podospora anserina. *Genome Biology* **9**, R77 (2008).

18 Bieszke, J. A. *et al.* The nop-1 gene of Neurospora crassa encodes a seven transmembrane helix retinal-binding protein homologous to archaeal rhodopsins. *Proc Natl Acad Sci U S A* **96**, 8034-8039 (1999).

19 Waschuk, S. A., Bezerra, A. G., Shi, L. & Brown, L. S. Leptosphaeria rhodopsin: Bacteriorhodopsin-like proton pump from a eukaryote. *Proceedings of the National Academy of Sciences of the United States of America* **102**, 6879-6883, doi:10.1073/pnas.0409659102 (2005).

20 Tateno, M., Ihara, K. & Mukohata, Y. The novel ion pump rhodopsins from Haloarcula form a family independent from both the bacteriorhodopsin and archaerhodopsin families/tribes. *Arch Biochem Biophys* **315**, 127-132 (1994).

21 Beja, O. *et al.* Bacterial rhodopsin: evidence for a new type of phototrophy in the sea. *Science* **289**, 1902-1906 (2000).

22 Wang, W. W., Sineshchekov, O. A., Spudich, E. N. & Spudich, J. L. Spectroscopic and photochemical characterization of a deep ocean proteorhodopsin. *J Biol Chem* **278**, 33985-33991 (2003).

23 Tsunoda, S. P. *et al.* H+ -pumping rhodopsin from the marine alga Acetabularia. *Biophys J* **91**, 1471-1479 (2006).

24 Han, X. & Boyden, E. S. Multiple-color optical activation, silencing, and desynchronization of neural activity, with single-spike temporal resolution. *PLoS ONE* **2**, e299 (2007).

25 Rudiger, M., Haupts, U., Gerwert, K. & Oesterhelt, D. Chemical reconstitution of a chloride pump inactivated by a single point mutation. *Embo J* **14**, 1599-1606 (1995).

26 Rudiger, M. & Oesterhelt, D. Specific arginine and threonine residues control anion binding and transport in the light-driven chloride pump halorhodopsin. *Embo J* **16**, 3813-3821 (1997).

27 Sato, M. *et al.* Ser-130 of Natronobacterium pharaonis halorhodopsin is important for the chloride binding. *Biophysical Chemistry* **104**, 209-216 (2003).

28 Sato, M. *et al.* Roles of Ser130 and Thr126 in chloride binding and photocycle of pharaonis halorhodopsin. *Journal of biochemistry* **134**, 151-158 (2003).

29 Kolbe, M., Besir, H., Essen, L. O. & Oesterhelt, D. Structure of the light-driven chloride pump halorhodopsin at 1.8 A resolution. *Science* **288**, 1390-1396 (2000).

30 Mogi, T., Marti, T. & Khorana, H. G. Structure-function studies on bacteriorhodopsin. IX. Substitutions of tryptophan residues affect protein-retinal interactions in bacteriorhodopsin. *J Biol Chem* **264**, 14197-14201 (1989).

31 Mogi, T., Stern, L. J., Chao, B. H. & Khorana, H. G. Structure-function studies on bacteriorhodopsin. VIII. Substitutions of the membrane-embedded prolines 50, 91, and 186: the effects are determined by the substituting amino acids. *J Biol Chem* **264**, 14192-14196 (1989).

32 Mogi, T., Stern, L. J., Hackett, N. R. & Khorana, H. G. Bacteriorhodopsin mutants containing single tyrosine to phenylalanine substitutions are all active in proton translocation. *Proc Natl Acad Sci U S A* **84**, 5595-5599 (1987).

33 Mogi, T., Stern, L. J., Marti, T., Chao, B. H. & Khorana, H. G. Aspartic acid substitutions affect proton translocation by bacteriorhodopsin. *Proc Natl Acad Sci U S A* **85**, 4148-4152 (1988).

34 Greenhalgh, D. A., Farrens, D. L., Subramaniam, S. & Khorana, H. G. Hydrophobic amino acids in the retinal-binding pocket of bacteriorhodopsin. *J Biol Chem* **268**, 20305-20311 (1993).

35 Han, X. *et al.* Millisecond-Timescale Optical Control of Neural Dynamics in the Nonhuman Primate Brain. *Neuron* **62**, 191-198 (2009).

36 Hofherr, A., Fakler, B. & Klocker, N. Selective Golgi export of Kir2.1 controls the stoichiometry of functional Kir2.x channel heteromers. *Journal of cell science* **118**, 1935-1943 (2005).

37 Stockklausner, C. & Klocker, N. Surface expression of inward rectifier potassium channels is controlled by selective Golgi export. *J Biol Chem* **278**, 17000-17005 (2003).

38 Kim, S. J., Mitra, D., Salerno, J. R. & Hegde, R. S. Signal sequences control gating of the protein translocation channel in a substrate-specific manner. *Developmental cell* **2**, 207-217 (2002).

39 Han, X. *et al.* Millisecond-timescale optical control of neural dynamics in the nonhuman primate brain. *Neuron* **62**, 191-198 (2009).

40 Lin, Y. *et al.* Activity-dependent regulation of inhibitory synapse development by Npas4. *Nature* **455**, 1198-1204 (2008).

41 Lin, J. Y., Lin, M. Z., Steinbach, P. & Tsien, R. Y. Characterization of engineered channelrhodopsin variants with improved properties and kinetics. *Biophys J* **96**, 1803-1814 (2009).

42 Bevensee, M. O. & Boron, W. F. in *pH and brain function* eds Kai Kaila & Bruce R. Ransom) Ch. 8, 129-152 (Wiley-Liss, 1998).

43 Boyden, E. S. & Raymond, J. L. Active reversal of motor memories reveals rules governing memory encoding. *Neuron* **39**, 1031-1042 (2003).

44 Bernstein, J. *et al.* in *Optical Interactions with Tissue and Cells XIX.* (ed Steven L. Jacques; William P. Roach; Robert J. Thomas) 68540H:68541-68511 (Proceedings of the SPIE).

45 Yaroslavsky, A. N. *et al.* Optical properties of selected native and coagulated human brain tissues in vitro in the visible and near infrared spectral range. *Physics in medicine and biology* **47**, 2059-2073 (2002).

46 Binzoni, T., Leung, T. S., Gandjbakhche, A. H., Rufenacht, D. & Delpy, D. T. The use of the Henyey-Greenstein phase function in Monte Carlo simulations in biomedical optics. *Physics in medicine and biology* **51**, N313-322 (2006).

47 Wang, L., Jacques, S. L. & Zheng, L. MCML--Monte Carlo modeling of light transport in multi-layered tissues. *Computer methods and programs in biomedicine* **47**, 131-146 (1995).

48 Bernstein, J. G. *et al.* Prosthetic systems for therapeutic optical activation and silencing of genetically-targeted neurons. *Proceedings - Society of Photo-Optical Instrumentation Engineers* **6854**, 68540H (2008).